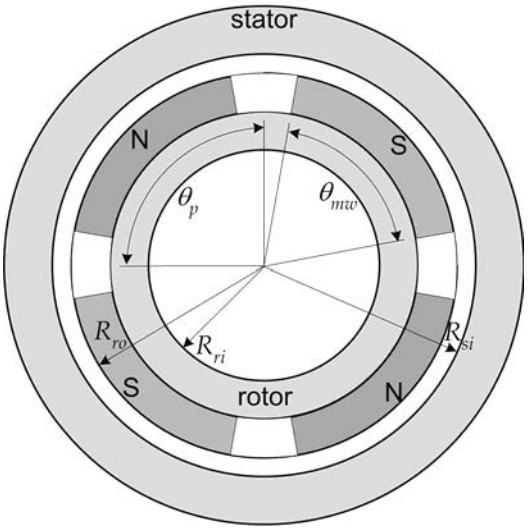

Figure 6-1. A rotor having surface mounted magnets.

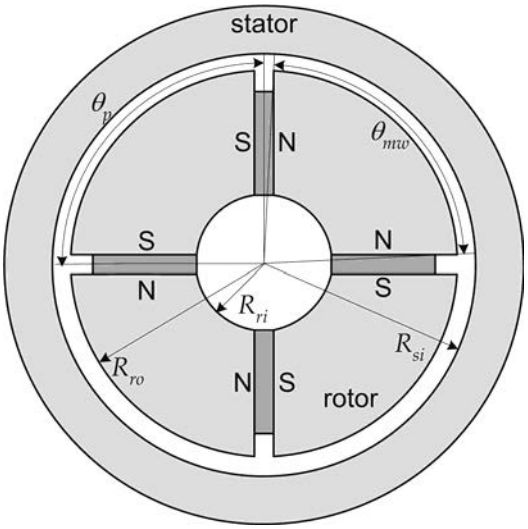

Figure 6-2. A rotor having spoke magnets.

When $N_p = 1$, the fundamental $n = 1$ term must be computed using (B.32) through (B.35). The terms K_{rn} and $K_{\theta n}$ in the above equations are the radial and tangential Fourier series coefficients of the magnetization as described in (B.6) and illustrated in Appendix B.6.

6.2 Interior Permanent Magnet Rotors

Interior permanent magnet rotors appear in two common configurations. The spoke or circumferential magnet configuration is shown in **Fig. 6-2** and the stand-

ard buried or radial magnet configuration is shown in **Fig. 6-3**. While both of these configurations can operate at speeds greater than surface magnet rotors, they are commonly used for distinctly different applications. The spoke configuration promotes flux concentration when the cross sectional area of the face of a pair of magnets is larger than the cross sectional area of the air gap they provide flux to. In this case, the air gap flux density can be greater than the remanence B_r of the permanent magnets, thereby permitting use of lower grade permanent magnet material. Secondly, the ferromagnetic material at the air gap in the spoke configuration can be tapered so that the air gap increases as one moves away from the center of the magnetic pole. Doing so allows one to tailor the air gap flux density distribution. In most cases, the goal is to create a sinusoidal flux density distribution.

In contrast to the spoke configuration, the standard buried magnet configuration is underexcited, *i.e.*, the flux concentration factor is inherently less than one. In addition, the rotor ferromagnetic material is one piece and therefore is inherently strong at high speeds. The air passages at each end of the magnets operate as flux barriers to minimize the amount of permanent magnet flux that travels around the magnet through the flux bridge region, rather than crossing the air gap. In fact, it is necessary that the flux bridge ferromagnetic material saturate magnetically. If it does not, no magnetic field crosses the air gap as shown in **Fig. 6-4** and the motor produces no mutual torque. When the flux bridge saturates as it does for all real world ferromagnetic materials, flux crosses the air gap into the stator as shown in **Fig. 6-5**.

In addition to the standard buried magnet configuration shown in Fig. 6-3, it is possible to use two magnets per rotor magnet pole as is done in the spoke configuration, but include flux bridges as used in the buried magnet configuration. This

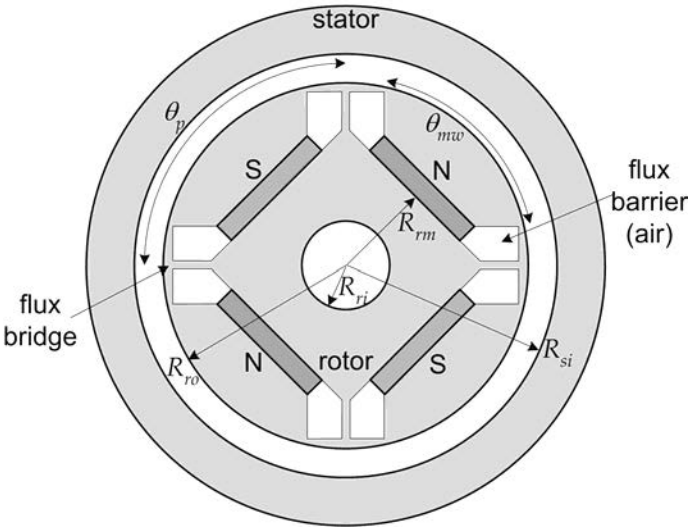

Figure 6-3. A rotor having buried magnets.

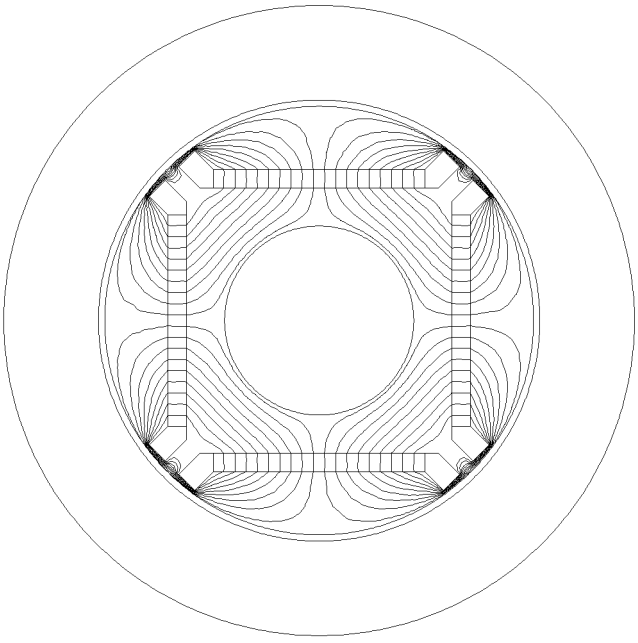

Figure 6-4. Flux flow in a rotor having buried magnets in ideal nonsaturating ferromagnetic material.

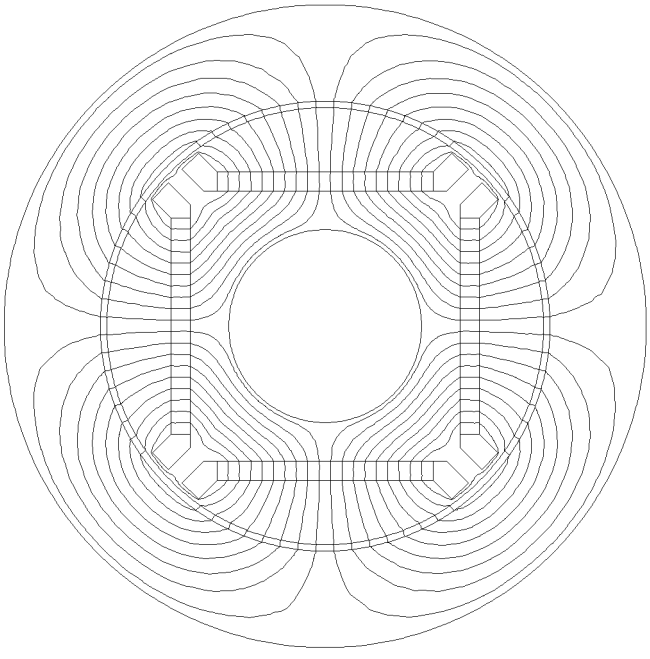

Figure 6-5. Flux flow in a rotor having buried magnets in saturating ferromagnetic material.

alternative buried magnet configuration offers the flux concentration of the spoke magnet configuration and the one piece rotor construction of the buried magnet configuration. The characteristics of this configuration closely follow that of the standard buried magnet configuration that is considered in what follows.

Based on these characteristics, the standard buried magnet configuration does not appear to offer much promise as a high performance motor. However, this motor can produce substantial reluctance torque as described by the first term in (3.37) since it is possible to create a sizable variation in the air gap inductance. In summary, the buried magnet configuration is generally most useful when constructed to produce both mutual and reluctance torque.

Spoke Magnet Configuration

With simplifying assumptions, it is possible to find the air gap flux density for the spoke magnet configuration by solving the appropriate partial differential equation. The simplifying assumptions include a requirement of having a constant air gap length. Since varying the air gap length over a rotor pole is a strength of the spoke magnet configuration, the air gap flux density is best approximated using a magnetic circuit solution approach.

Consider the example magnetic flux flow pattern shown in the spoke magnet motor shown in **Fig. 6-6**. Each permanent magnet provides one half the air gap flux over one rotor pole. The ferromagnetic rotor pole sections have a smaller radius than the overall rotor radius. As a result, the air gap length varies over the

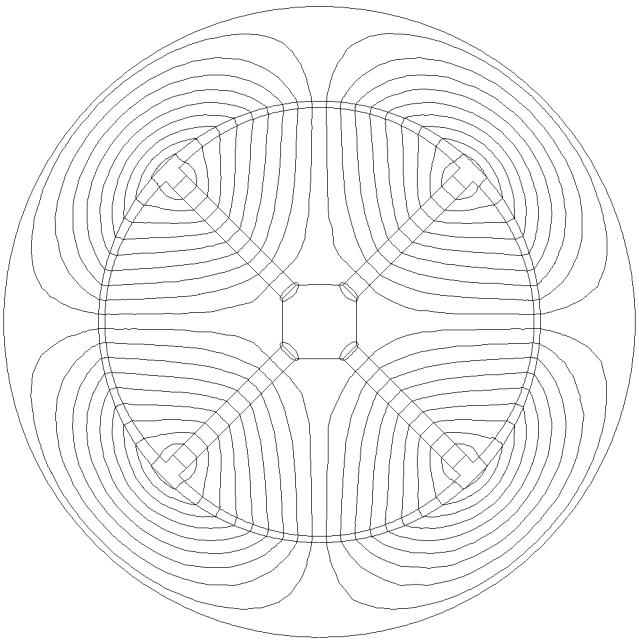

Figure 6-6. Flux flow in a rotor having spoke magnets.

rotor pole, with the minimum appearing at the pole center, and the resulting air gap flux density decreases as one moves away from the magnet center. Leakage flux flowing from one side of each permanent magnet to the opposite side is clearly demonstrated in the nonferromagnetic region at the inner rotor radius. Though not shown because of insufficient finite element resolution, leakage flux also flows from one side of each permanent magnet to the other in the air region radially beyond each permanent magnet near the outside rotor radius.

Because the flux paths repeat for every permanent magnet, the air gap flux density can be found by considering the magnetic flux from any one magnet. **Figure 6-7** illustrates a magnetic circuit model for one such magnetic flux path. In the figure, ϕ_r and R_m are the permanent magnet flux source and magnet reluctance respectively. R_r and R_s are the respective reluctances of the rotor and stator ferromagnetic areas. The reluctance R_l models the combined leakage flux paths at the inner and outer radii of the permanent magnet. Because magnetic flux from one magnet flows through one half the air gap cross sectional area, $2R_g$ is the reluctance of each half air gap cross section.

As was done in Chapter 4, it is convenient to simplify the magnetic circuit in Fig. 6-7 as shown in **Fig. 6-8** before solving for the air gap flux ϕ_g. In Fig. 6-8*a*, the rotor and stator ferromagnetic reluctances are combined as are the two air gap reluctances. If desired, the leakage reluctance R_l can be modeled using the circular-arc, straight-line technique described in Chapter 2. In Fig. 6-8*a*, the leakage reluctance is combined with the magnet reluctance R_m and its effect is taken into account by the leakage factor K_l. Because reluctances add in parallel the same way that electrical resistances do, the leakage factor can be written as

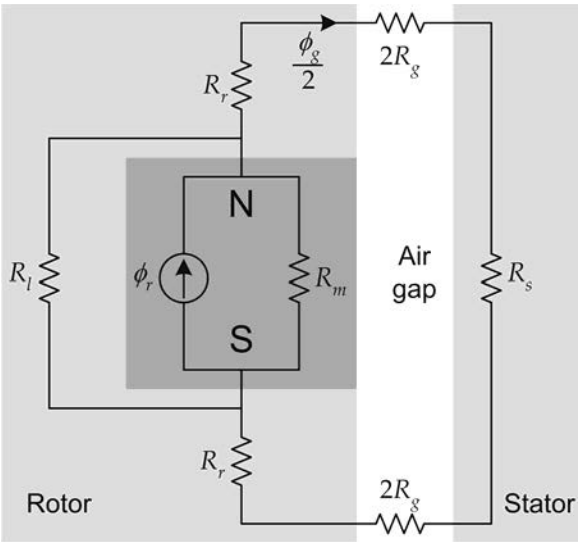

Figure 6-7. Magnetic circuit model for the spoke magnet configuration.

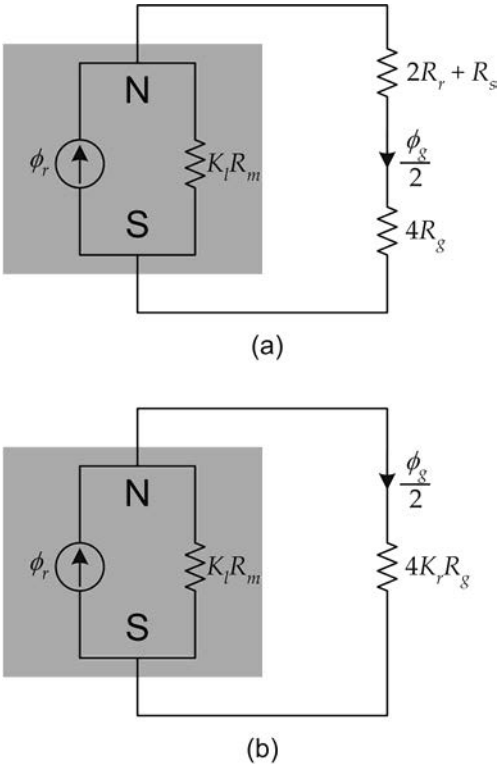

Figure 6-8. Simplification of the magnetic circuit model shown in Fig. 6-7.

$$K_l = \frac{R_l}{R_l + R_m} = \frac{1}{1 + \frac{R_m}{R_l}} \tag{6.3}$$

Since the leakage flux is small compared to the magnet flux, the leakage reluctance is typically much larger than the magnet reluctance, *i.e.*, $R_l \gg R_m$. Therefore based on (6.3), the leakage factor is close to but less than one, *e.g.*, $0.9 < K_l < 1.0$. In the ideal case where there is no leakage flux, R_l is infinite and $K_l = 1$.

The magnetic circuit is further simplified in Fig. 6-8*b* where the influence of the ferromagnetic portions of the rotor and stator are taken into account by a reluctance factor K_r. This factor is typically slightly larger than one, *e.g.*, $1.0 < K_r < 1.2$, and represents the relative amount the air gap reluctance must increase to compensate for the missing rotor and stator reluctances. As stated in Chapter 4, it is difficult to analytically determine the value of the reluctance factor, so its value is often chosen based on the experience of the designer.

Given the magnetic circuit in Fig. 6-8*b*, the air gap flux can be expressed using flux division as

$$\phi_g = \frac{2K_l R_m}{K_l R_m + 4K_r R_g}\phi_r = \frac{2\phi_r}{1 + \frac{4K_r R_g}{K_l R_m}} \tag{6.4}$$

Substituting the expressions in (4.2) for the magnet and air gap reluctances, the flux density relationships $B_g = \phi_g / A_g$ and $B_r = \phi_r / A_m$, and defining the flux concentration factor as

$$C_\phi = \frac{2A_m}{A_g} \tag{6.5}$$

because two magnets provide the air gap flux over one rotor pole pitch, (6.4) can be rewritten to give the air gap flux density as

$$B_g = \frac{C_\phi}{1 + \frac{2K_r \mu_R g}{K_l l_m} C_\phi} B_r \tag{6.6}$$

To visualize this expression, **Fig. 6-9** illustrates the ratio B_g/B_r versus the flux concentration factor C_ϕ using the typical parameter values $K_r = 1.1$, $K_l = 0.95$, $\mu_R = 1.05$ and $l_m/g = 4$. For these parameter values the flux concentration factor must be greater than approximately 2.5 for the air gap flux density to be greater than the

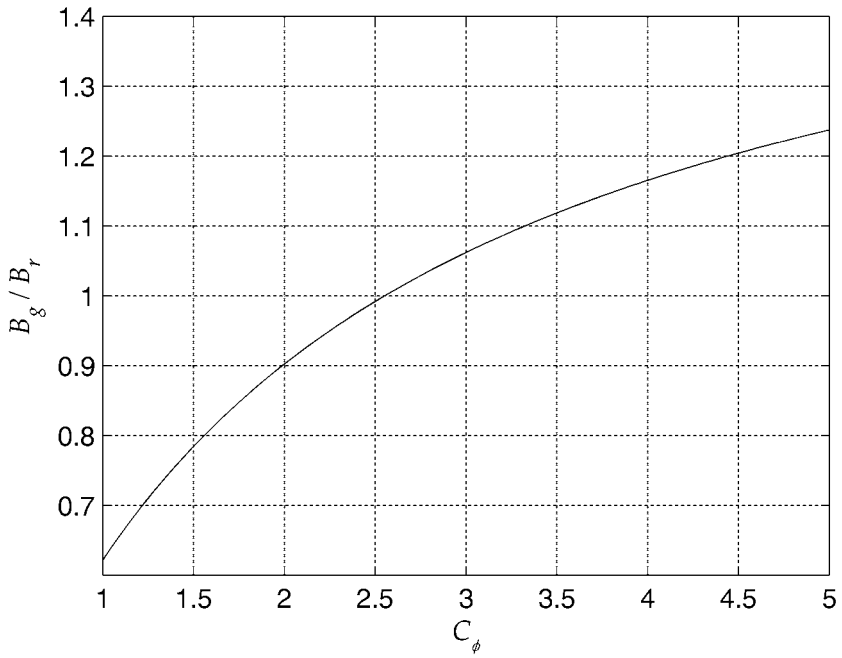

Figure 6-9. Normalized air gap flux density for the spoke magnet configuration.

permanent magnet remanence B_r. Flux concentration factor values greater than 2.5 are easily achieved as the rotor radius or the number of magnet poles increases.

The air gap flux density in (6.6) is an approximation to the flux density over the surface of the rotor magnetic pole having angular width θ_{mw}. When the air gap length varies over the rotor magnetic pole, *i.e.*, $g = g(\theta)$, (6.6) describes the resulting variation in flux density as a function of position. If $\theta = 0$ is the pole center, then beyond the ends of the rotor pole, $|\theta| > \theta_{mw}/2$, the flux density crossing into the stator decreases in amplitude and reaches zero at the midpoint between rotor magnetic poles at $\theta = \pm\theta_p/2$. Over the adjacent rotor magnetic poles, the flux density changes sign denoting flux traveling in the opposite direction. The exact transition shape from the value given in (6.6) at $\theta = \pm\theta_{mw}/2$ to $B_g = 0$ at $\theta = \pm\theta_p/2$ is difficult to determine with certainty. Based on finite element analysis, it is common to start the transition from the value given in (6.6) at least one air gap length before reaching $\theta = \pm\theta_{mw}/2$. A smooth curve is then fit between that initial point to $B_g = 0$ at $\theta = \pm\theta_p/2$. The exact shape of this curve is not highly critical since it typically has much greater influence over the higher harmonics of the air gap flux density than it does over the fundamental harmonic.

To illustrate (6.6) versus position, consider **Fig. 6-10**. Using typical parameter values, this figure shows the air gap flux density over a North and South pole pair. The shaded lines mark the rotor magnetic pole edges. Two transition shapes starting one air gap length before the rotor magnetic pole edges are shown. The solid lines illustrate a linear transition, whereas the dashed line illustrates the use of one

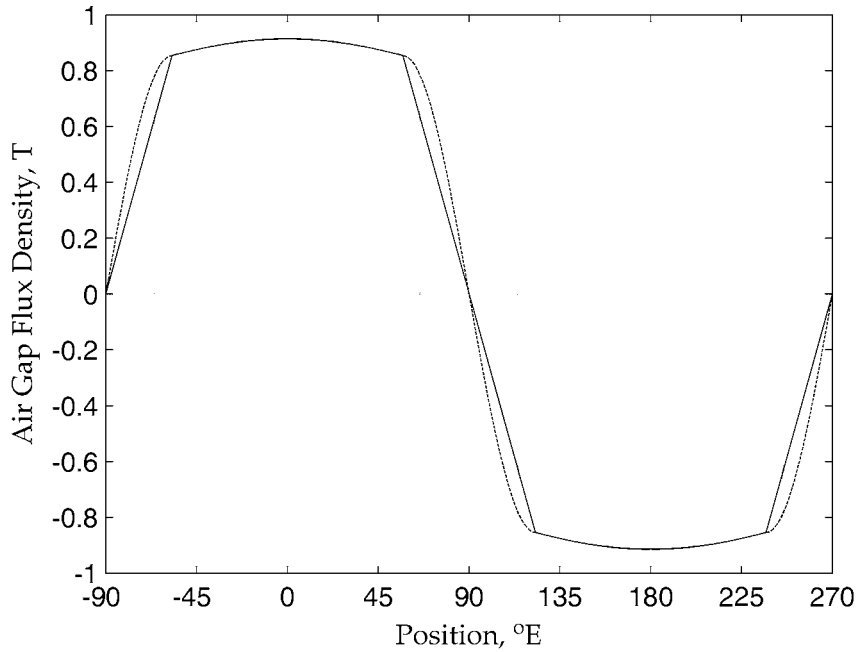

Figure 6-10. Air gap flux density distributions for the spoke magnet configuration.

quarter period of a sinusoid to create a smoother transition to zero. In both cases, the air gap flux density decreases as one moves away from the pole centers because the air gap length was doubled between the pole center and the outer pole edges. This demonstrates how the rotor ferromagnetic material can be shaped to tailor the air gap flux density. The closeness of the two flux density curves confirms that the chosen transition shape does not play as significant a role as the placement of the transition region starting point.

Using samples of one electrical period of the air gap flux density, the Fourier series coefficients for the Fourier series representation in (6.1) can be found using the procedure given in Appendix A.

Buried Magnet Configuration

As with the spoke magnet configuration, magnetic circuit analysis is useful for approximating the air gap flux density distribution for the buried magnet configuration. However, in the buried magnet configuration, the analysis is complicated by the high magnetic saturation in the flux bridge area in Fig. 6-3 and in the finite element analysis flux plot in Fig. 6-5.

Based on the magnetic flux plot in Fig. 6-5, **Fig. 6-11** depicts a magnetic circuit model for one flux loop modeling one half of two magnets and the associated flux paths. In the figure, $2R_g$ is the reluctance of one half of the air gap over one rotor pole, R_{rt} and R_{rb} are reluctances of the rotor ferromagnetic sections on top and bottom of the permanent magnet respectively. R_s is the reluctance of the stator. R_l is the reluctance of the flux leakage path through the flux barriers and R_b is the nonlinear, saturated reluctance of the flux leakage path through the flux bridge. The two permanent magnets shown are one half the corresponding rotor magnets.

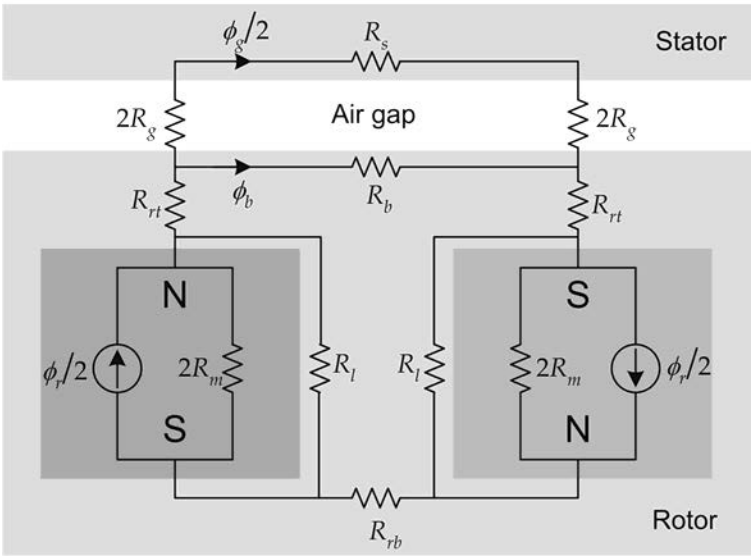

Figure 6-11. Magnetic circuit model for the buried magnet configuration.

The air gap flux ϕ_g and the flux bridge flux ϕ_b in Fig. 6-11 are of particular importance. To solve for these fluxes, it is convenient to simplify the circuit as shown in **Fig. 6-12**. In Fig. 6-12*a*, the rotor ferromagnetic reluctances are combined into one reluctance R_r and the leakage reluctances R_l are absorbed into the magnet reluctances by the inclusion of a leakage factor K_l, which is very close to, but less

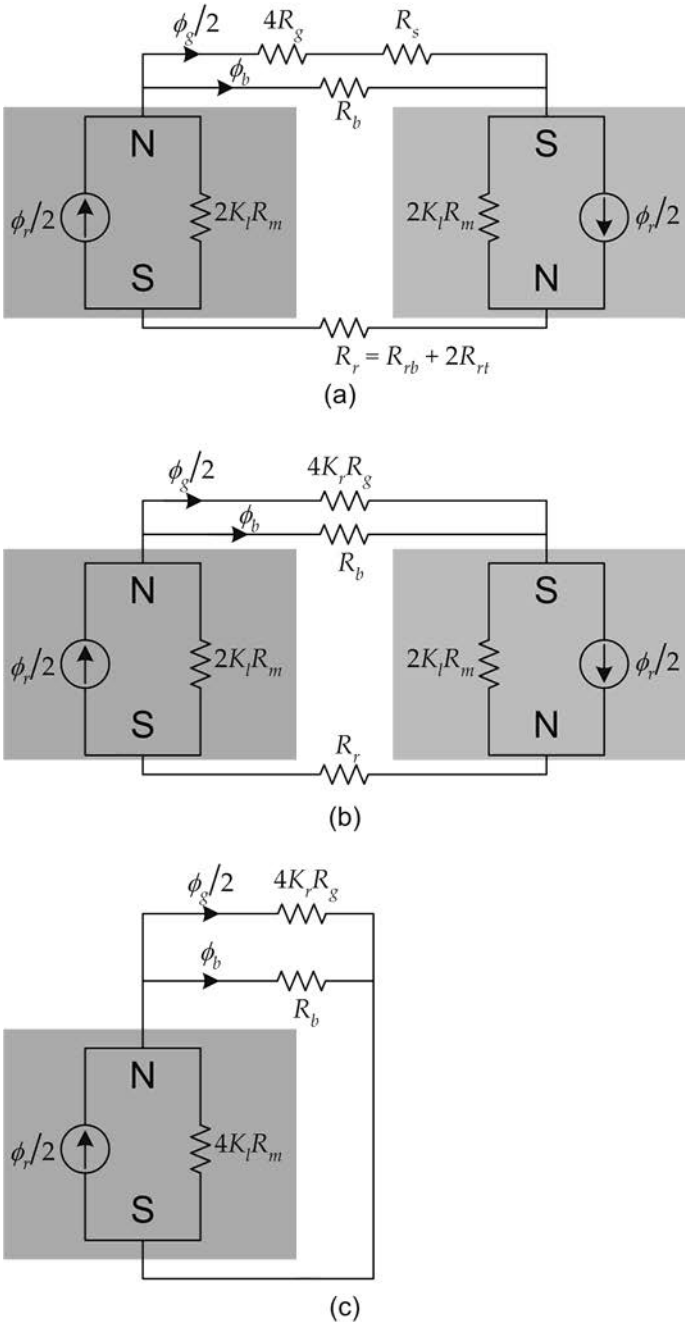

Figure 6-12. Simplification of the magnetic circuit model shown in Fig. 6-11.

than one. The stator reluctance is combined with the air gap reluctance in Fig. 6-12*b* and is taken into account by the reluctance factor K_r, which is close to, but greater than one. The leakage factor and reluctance factors fulfill the same role here that they do in surface magnet and spoke magnet rotors. Finally, in Fig. 6-12*c*, the rotor reluctance R_r is eliminated because it is very small compared to R_b and $4K_rR_g$ and also because it has no effect on the division of flux between ϕ_g and ϕ_b. With the elimination of the rotor reluctance, the two half magnets are combined to make one magnet of twice the length. This simply doubles the magnet reluctance as shown.

Using flux division, *i.e.*, flux divides just as current does between parallel resistances, the air gap flux ϕ_g can be written as

$$\phi_g = \frac{\dfrac{1}{4K_rR_g}\phi_r}{\dfrac{1}{4K_rR_g}+\dfrac{1}{R_b}+\dfrac{1}{4K_lR_m}} = \frac{\phi_r}{1+\dfrac{4K_rR_g}{R_b}+\dfrac{K_rR_g}{K_lR_m}} \tag{6.7}$$

Substituting the flux density relationships $B_g = \phi_g/A_g$ and $B_r = \phi_r/A_m$, and using the flux concentration factor defined as $C_\phi = A_m/A_g$, (6.7) can be rewritten to describe the air gap flux density B_g as

$$B_g = \frac{C_\phi}{1+4K_r\left(\dfrac{R_g}{R_b}+\dfrac{R_g}{K_lR_m}\right)}B_r \tag{6.8}$$

In defining the flux concentration factor as $C_\phi = A_m/A_g$, one must choose a value for the air gap cross sectional area A_g. Since very little flux crosses the air gap over the flux bridges, setting this area equal to the total air gap area over one pole, *i.e.*, $A_g = R_{ro}\theta_p L_{st}$ where L_{st} is the axial stack length, overestimates the actual area through which the air gap flux flows. A better estimate uses the angular magnet pole width θ_{mw}, *i.e.*, $A_g = R_{ro}\theta_{mw}L_{st}$.

The term R_g/R_b in the denominator of (6.8) is the ratio of the air gap reluctance to the flux bridge reluctance. This ratio must be small for significant flux to cross the air gap. Alternatively, the inverse ratio R_b/R_g must be large. That is, the flux bridge must be much more reluctant to the passage of magnetic flux than the air gap. When this is true, the majority of the permanent magnet flux will cross through the air gap rather than through the flux bridge.

The last term in the parentheses in the denominator of (6.8) can be rewritten by substituting the expressions in (4.2) for the magnet and air gap reluctances. In doing so, (6.8) becomes